Journal of Experimental Pharmacology

Dovepress
Taylor & Francis Group

Open Access Full Text Article

ORIGINAL RESEARCH

Biocompatibility and Effectiveness of Amphotericin B-Loaded Metal-Organic Structures (AmB-ZIF-8) as Dermal Drug Transporters in Experimental Cutaneous Leishmaniasis

Heider Carreño[1], Jorge Osorio[1], Enrique Mejía-Ospino[2], Patricia Escobar[1]

[1]Centro de Investigación de enfermedades tropicales (CINTROP-UIS), Departamento de Ciencias Básicas, Escuela de Medicina, Universidad Industrial de Santander, Bucaramanga, Colombia; [2]Laboratorio de Espectroscopia Atómica Y Molecular (LEAM), Escuela de Química, Universidad Industrial de Santander, Bucaramanga, 680002, Colombia

Correspondence: Patricia Escobar, Centro de Investigación de enfermedades tropicales (CINTROP-UIS), Departamento de Ciencias Básicas, Escuela de Medicina, Universidad Industrial de Santander, Bucaramanga, Colombia, Email pescobar@uis.edu.co

Purpose: Information on metal-organic frameworks (MOFs) as topical drug delivery systems (DDS) for antileishmanial drugs is limited. This study outlines our strategies for developing MOF-drug conjugate as a topical treatment for cutaneous leishmaniasis (CL) in mice infected with *Leishmania (L). amazonensis*.

Methods: We selected conjugates from two commercial MOFs (ZIF-8 and Fe-BTC) and seven antileishmanial compounds. Amphotericin B (AmB) and zeolitic imidazolate framework-8 (AmB@ZIF-8) were chosen and prepared at an AmB: ZIF-8 ratio of 1.5:1.0 using the impregnation method. Conjugates were characterised using dynamic light scattering, UV-Vis, FTIR, and SEM. Hydrogels were prepared and evaluated for toxicity and efficacy in CL-BALB/c mice.

Results: AmB@ZIF-8 exhibited a 59.6% loading capacity, 6.67% encapsulation efficiency, and 2% in vitro drug release (IVR). The particle size of AmB@ZIF-8 was smaller and more polydisperse than ZIF-8 (1370 nm vs 2537 nm). The conjugation of AmB to ZIF-8 was demonstrated. AmB@ZIF-8 exhibited similar antileishmanial activity to AmB against promastigotes. Topical 0.5% AmB@ZIF-8 and 0.5% AmB hydrogels, administered for 30 days, were unable to decrease lesion sizes or parasite loads. Initially, there was stabilisation of the lesion size; however, the lesions subsequently increased considerably during the 30-day follow-up period. The MOF-hydrogel treatment was non-irritating.

Conclusion: There were very low EE% and AmB IVR. AmB@ZIF-8 and AmB hydrogels were found to be safe but ineffective against CL-infected mice. Several factors may explain these negative results, including the large size of the commercial ZIF-8, the aggregation of AmB in solution, the excess AmB used for impregnation, and the conditions of the IVR assay. We suggest continuing to use ZIF-8 as a DDS due to its sensitivity to acidic pH levels; however, we recommend reducing the particle size and lowering the drug-to-ZIF-8 ratio. Other alternatives are discussed in the present paper. We also advocate investigating alternative antileishmanial drugs as cargo, such as miltefosine or pentamidine.

Keywords: *Leishmania amazonensis*, metal-organic structures, drug delivery systems, skin toxicity, amphotericin B, experimental cutaneous leishmaniasis

Introduction

Cutaneous leishmaniasis (CL) is a significant public health concern in countries where it is endemic. It involves vectors, parasite species, reservoirs, and geographically endemic areas. The World Health Organization (WHO) classifies CL as an emerging, uncontrolled, and neglected tropical disease.[1] It is estimated that there are 600,000 to 1 million new cases of cutaneous leishmaniasis (CL) annually worldwide. This disease is caused by over 15 species of *Leishmania* protozoan parasites, which are transmitted by infected sandflies.[1] Localised CL typically presents as skin ulcers on exposed body parts. These ulcers can heal spontaneously, leaving lifelong and stigmatised scars or spreading to other skin areas or

Received: 28 December 2024
Accepted: 17 April 2025
Published: 30 May 2025

Graphical Abstract

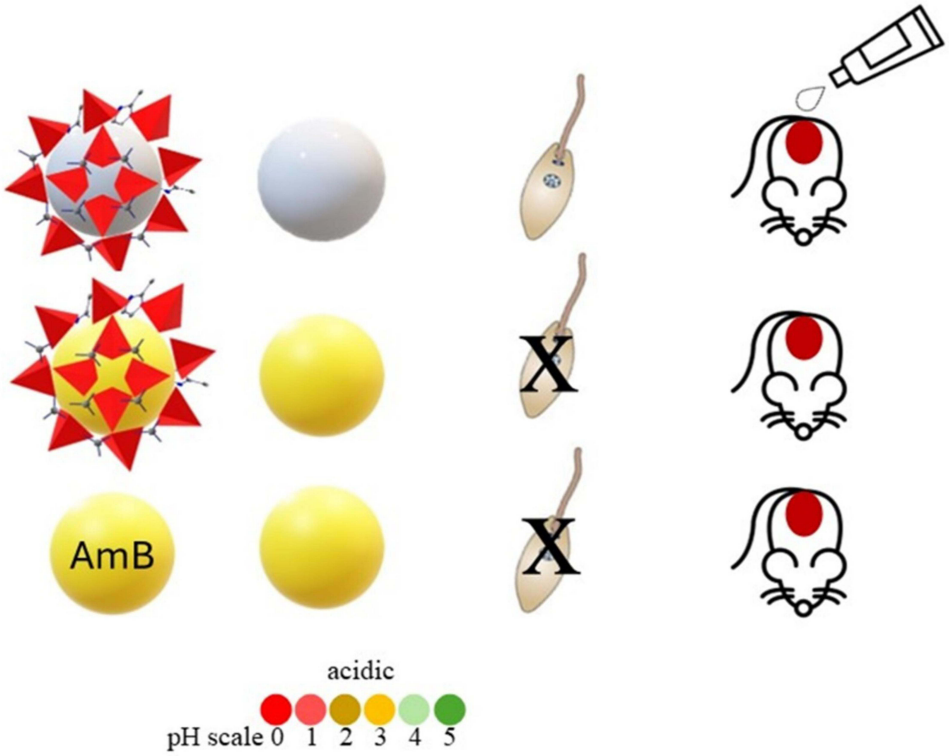

mucous membranes.[2] There are no vaccines, and the few and old available treatments, if accessible, could be toxic, painful, or ineffective. Systemic treatments may include oral miltefosine, intramuscular pentamidine isethionate (PMD), and intramuscular or intravenous Sb^V administration. Liposomal amphotericin B (L-AmB) is the rescue drug used for non-responsive patients, pregnant women, HIV-coinfected patients, and complicated patients with disseminated or diffuse CL.[3] The recommended localised treatment for American CL includes intralesional pentavalent antimonial (Sb^V), local thermotherapy, and topical paromomycin (PAR) cream.[3] Topical treatments are a practical and cost-effective approach with a lower toxicity risk than systemic treatment.[2] Systemic drugs have been reformulated into topical or intralesional formulations and tested on humans and experimental models. The results varied depending on the drug used, the dose, formulation type, and the parasite species.[1,4–7] These drugs have also been encapsulated in topical drug delivery systems (DDS) to improve dermal drug penetration, macrophage localisation, and antileishmanial efficacy while decreasing toxic effects.[8–13] Various topical DDS include ultra deformable and nanoliposomes, lipid colloidal drug carriers such as nano and microemulsions (NE), solid lipid nanoparticles (SLN), and nanostructured lipid carriers (NLC), metallic nanoparticles, and polymeric nanoparticles like poly(lactide-co-glycolide) (PLGA) and poly (glycolic acid) (PGA).[8–13]

Recent advancements in biomedicine and cosmetics have revealed the potential use of metal−organic structures (MOFs) as effective drug carriers for treating skin diseases.[14,15] MOFs are porous, flexible, and easily adjustable materials resulting from the coordinated interaction of cationic metal groups (Zn2+, Ag2+, Al3+, Fe3+, Zr4+) with organic ligands based on carboxylic acid, imidazole, and pyridine.[16] Due to their structural characteristics of high porosity (ranging from 0.4 to 6 nm), extensive surface area, and tunable pore sizes, MOFs demonstrate significantly greater cargo-loading efficiency. This includes various diverse molecules, such as antimicrobial, antiviral, anticancer drugs, metabolic labelling molecules, hormones, lipids, and nucleic acids.[17,18] They also exhibit low cytotoxicity, high biodegradability, and excellent biocompatibility. Diverse drugs (structurally, physiochemically, or pharmacologically)

have been tested as cargoes with various types of MOFs, such as Fe-MOFs (MIL-100 and MIL-127), Zr-MOFs (UiO-66), and Zn-MOFs (ZIF-8).[15,19–21]

MOFs have primarily been proposed for intravenous administration; however, intriguing applications, such as gels, creams, ointments, patches, or innovative composite carriers, exist for cutaneous and transdermal use.[22–24] For instance, to address the local delivery of insoluble drugs, composite carriers integrated with cyclodextrin (CD)-MOF and CD-nanosponge (used for bio-adhesion) have shown improved in vitro release and transdermal permeation.[23] Some composite patches made from biopolymers containing MIL-100 and MIL-127 (Fe) nano-MOF, along with one or more drugs (caffeine, ibuprofen, azelaic acid, and nicotinamide), demonstrated high drug-loading capacities and enabled controlled and sustained drug release through porcine skin.[15,25] The encapsulation rate and skin permeation may depend on the physicochemical and structural properties of MOFs, such as flexibility, organic linker H-donor capacity, and polarity, as well as the properties of the drugs themselves, including lipophilicity and molecular weight. Furthermore, maintaining a hydrophobic-hydrophilic balance between the selected MOF and the cargo is crucial due to the polar and non-polar components of the MOF, including metal clusters and aromatic ligands.[14] These results underscore the importance of rationally selecting the MOF candidates. For example, when testing various MOF platforms for the topical delivery of salicylic acid, one of the UiO-66-NH2 platforms showed a higher drug load and improved drug release under simulated cutaneous conditions.[22]

Limited information exists regarding the use of MOFs as a topical drug delivery system for treating cutaneous leishmaniasis (CL).[26] Nevertheless, applying topical formulations that incorporate MOFs and antileishmanial drugs directly onto CL lesions may facilitate controlled drug release into the deeper skin layers, where the parasites reside within infected dermal macrophages. Considering the potential of MOFs as transdermal drug delivery systems, alongside the limited availability of antileishmanial drugs and the systemic toxicity associated with injectable and oral medications, designing topical treatment options using available antileishmanial medicines (drug repositioning) presents a viable and promising short-term alternative.[27]

This study outlines our strategies for developing a drug@MOF conjugate as a potential drug delivery device (DDD). We selected a commercial MOF and an antileishmanial drug for loading. They were characterised in terms of physicochemical, spectroscopic, and pharmacological properties. Subsequently, topical hydrogel formulations of 1% Carbopol-950 containing the conjugate and free components were prepared to assess their safety and antileishmanial activity in BALB/c mice with CL caused by *L. (L). amazonensis*.

Materials and Methods

Drugs and Compounds

Amphotericin B (AmB), ketoconazole (KTZ), paromomycin sulphate salt (PM), pentamidine diisethionate (PMD), potassium antimony (III) tartrate hydrate (Sb^{III}), quercetin, and curcumin were purchased from Sigma Chemical Company (St. Louis, MO, USA). Miltefosine (MTF) was purchased from Cayman (Michigan, USA), and dimethyl sulfoxide (DMSO) was obtained from Panreac, Darmstadt, Germany. The molecular weights and LogP values of the drugs and compound structures are detailed in Table S1. Ultrapure water (type I water) was obtained from the Milli-Q PLUS-PF purification system].

Commercial MOF and Reagents

Fe-BTC (iron 1,3,5-benzenetricarboxylate) and ZIF-8 (2-methylimidazole zinc) without salt) Under the commercial names Basolite F300 and Basolite Z1200, these materials were acquired from BASF (Sigma-Aldrich) without further purification (Table S2). N, N-dimethylformamide (DMF, 99.5%), triethylamine (TEA), triacetin (pH 5–6), DMSO, ethanol, and methanol were obtained from Sigma Aldrich.], For the hydrogels, Carbopol 940, sodium benzoate, and triethylamine (TEA) were acquired from Sigma-Aldrich.

In vitro Test on Parasites and Mammalian Cells

Parasites and Mammalian Cells

All parasites and cell lines used were obtained commercially from the American Type Culture Collection (ATCC) in Rockville, USA. Promastigotes of *L. amazonensis* (MHOM/BR/73/LV78) were cultured at 28 °C in Schneider's medium (Gibco, Grand Island, NY, USA), supplemented with 10% fetal calf serum (FCS) from Gibco. Human leukemia THP-1 cells were cultured in RPMI 1640 medium (Gibco) with 10% FCS at 37°C in a 5% CO_2/95% air mixture. THP-1 cells were transformed into the adherent phenotype with phorbol 12-myristate 13-acetate (PMA, Sigma-Aldrich, 130 nM) for 24 hours at 34 °C.

Stock-Solutions

The compounds were prepared in DMSO, except for MTF and PMD, which were diluted in PBS at pH 7.2. Fe-BTC and ZIF-8 were dispersed in DMSO and then sonicated using an ultrasonic processor (Cole-Parmer Instruments) at 20 hz and 15% amplitude for 1 min to achieve a final concentration of 2 mg/mL. Working solutions were prepared in culture medium at least one hour prior to the assays.

Antiparasitic and Cytotoxicity

Leishmania promastigotes and mammalian cells were incubated in triplicates with serial 1:3 dilutions of each compound for 72 hours. Control cells were incubated with medium alone. The drug's effectiveness against parasites was assessed using the resazurin reduction test. 20 µL of resazurin (0.11 mg/mL, Sigma-Aldrich) was added to each well. After four hours, the optical densities (OD) were measured at 570 and 600 nm using a Synergy H1 microplate reader from BioTek Instruments, Inc., VT, USA. The toxicity of compounds on THP-1 cells was evaluated using the MTT assay. Following treatment, 20 µL of MTT solution (2.5 mg/mL) was added to each well for 4 hours. The supernatant was removed, and insoluble formazan crystals were dissolved with 100 µL of DMSO. The absorbances were determined at 580 nm. Percentages of parasite inhibition or cell toxicities were calculated using the following formula: % parasite inhibition/% cell toxicity = 100*(OD control group−OD treated group) / OD control group. The 50% inhibitory concentration (IC_{50}) or cytotoxic concentration (CC_{50}) was determined using GraphPad Software, version 8.0, 2018. Three experiments were performed in triplicate (n = 9). The selectivity indexes (SIs) were calculated by dividing the drug's activity against cells by its activity against parasites (CC_{50} cells/IC_{50} parasites).

Cell Morphological Changes After MOF Treatment

THP 1 cells were placed on glass coverslips in a 24-well plate and differentiated with PMA as previously described. After that, they were incubated with 60 and 120 µg/mL of both MOFs and with medium alone for 24 hours. The cells were washed three times with PBS at pH 7.2, fixed with methanol, stained with Giemsa, and observed under a microscope to detect any morphological changes.

Fe-BTC and ZIF-8 MOFs Solubilities

Different quantities of MOFs (1−8 mg) were added to 2–3 mL of various solvents, including DMSO, triacetin, methanol, ethanol, type I water, and 1–10% Tween 20 or Tween 80 in phosphate-buffered saline (PBS) or distilled water, at pH 7.2. Samples were left at room temperature (RT) for 24 hours, stirred magnetically at 150 rpm for 1 hour at RT, or sonicated for 1 minute. In some experiments, samples were titrated with 0 to 240 µL of HCl or NaOH until solubilisation occurred. In a final experiment, MOFs were dispersed in DMSO, ethanol, and type I water at a final concentration of 1 mg/mL, sonicated for 1 minute, and then characterised for particle size, PDI, and final pH. Some samples were centrifuged at 10,000 rpm (16,000 g) for 10 minutes.

Preparation of AmB@ZIF-8, Drug Loading Capacity (DLC) and Encapsulation Efficiency (EE%)

AmB was loaded into ZIF-8 at a ratio of 1.5:1.0 using the solvent adsorption method with some modifications.[28] 30 mg of AmB was dispersed in 10 mL of methanol and stirred at 150 rpm for 30 minutes at RT. Subsequently, 20 mg of ZIF-8 was added to the mixture and magnetically stirred for 72 hours. The AmB@ZIF-8 mixture was then centrifuged at

10,000 rpm for 15 minutes and washed twice with methanol and Type I water to eliminate excess solvent. The resultant solid was dried under a vacuum at 200 °C overnight and stored in the refrigerator until use. The quantity of AmB loaded was determined by subtracting the mass of AmB in the supernatant from the total mass of AmB in the initial solution. The Drug Loading Capacity (DLC%) was calculated using the following equation: DLC% = 100 * (amount of AmB in ZIF-8) / (mg AmB total - mg AmB in the supernatant + mg ZIF-8). The Encapsulation Efficiency (EE%) was calculated as EE% = (mg AmB total – mg AmB free) / mg AmB total * 100. The unloaded AmB was assessed by placing 400 µL of ZIF-8@AmB at 1.3 mg/mL in DMSO in a Nanosep Centrifugal Device (Pall Corporation, Puerto Rico) and centrifuging at 10,000 rpm for 15 minutes at RT. The concentration of AmB capable of crossing the membrane was quantified. To quantify AmB, a calibration curve was established in DMSO using UV-Vis spectrophotometry at a wavelength of 416 nm. The AmB stock solution was prepared in DMSO at a concentration of 5 mg/mL, and working solutions were prepared at concentrations ranging from 1.25 to 300 µg/mL.

In vitro Release (IVR) Assay

To select the receptor medium for the IVR assay, we first evaluated the solubility of AmB by dissolving 1–2 mg of AmB in Tween 80 or Tween 20, in either PBS (pH 7.4) or distilled water with 10% DMSO. The mixtures were stirred for 72 hours. Subsequently, samples were centrifuged at 10,000 rpm for 10 minutes, and the concentration of AmB in the supernatant was measured using UV-Vis spectroscopy.

The IVR profile of AmB was assessed using SnakeSkin dialysis tubing (3.5 kDa MWCO, 16 mm diameter, Thermo Scientific, USA), which had been previously hydrated with PBS at pH 7.4 for 1 hour. Briefly, 2 mL of ZIF-8, AmB-free, or AmB@ZIF-8 at a concentration of 2 mg/mL in DMSO was placed inside the membranes. After sealing, the samples were submerged in a beaker containing 20 mL of the receptor solution (PBS at pH 7.4, 10% Tween 20, and 10% DMSO), and they were continuously stirred magnetically at 150 rpm and 25 °C. Samples of 300 µL were collected at various intervals (0.25, 0.5, 1, 2, 3, 4, 6, 7, 8, 9, 24, 26, 28, 30, 32, 48, and 96 hours) and analysed for AmB concentration. The volume withdrawn was immediately replaced with fresh solution. The data obtained were analysed to determine the cumulative amount of permeated drug in the recipient solution (µg) and plotted against the sampling time (hour).

Characterisation

Particle size (nm) and polydispersity index (PDI) were measured using dynamic light scattering (DLS) with a Malvern Zetasizer Nano ZS at RT. Experiments were run in triplicate. Samples were dispersed in different solvents (ultrapure water, ethanol, and DMSO) and sonicated using an ultrasound tip (20 KHz at 15% amplitude) for 1–3 minutes. Samples for the UV-VIS spectrum were dispersed in ultrapure water and DMSO at a concentration of 1 mg/mL using an ultrasound tip (15%, 1 minute). The absorption spectra (200 to 800 nm) of MOFs and AmB solutions were collected on a MultiSkan Go spectrophotometer at RT. To identify the functional chemical groups, infrared absorption measurements (ATR-FTIR) were recorded using a Nicolet iS50 Fourier-transform infrared spectrometer (Thermo Scientific, Waltham, MA, USA). Absorption spectra were obtained in the wavelength range of 400–4,000 cm^{-1} with a resolution of 4 cm^{-1} in attenuated total reflection (ATR) mode. Morphology was analysed by Field-emission scanning electron microscopy (SEM) using an EVO MA10 SEM (Carl Zeiss) at magnifications ranging from 5.00 to 10.00 kX, an acceleration voltage of 20 kV, and a working distance of 8.5 mm. The samples were previously coated with a thin layer of 5 nm gold, as recommended for non-conductive materials. This measurement was taken using a piezoelectric device that had been conditioned for use with spray equipment. Energy Dispersive X-ray spectroscopy (EDS) compositional analysis was performed using an X-Act detector (Oxford Instruments).

In vivo Studies

Hydrogels Preparations

The compounds were initially mixed with DMSO to formulate a hydrogel containing 1% ZIF-8, 0.5% AmB, and 0.5% AmB@ZIF-8. The composition of the final formulation is detailed in Table S3. Carbopol 940 (50 mg) and sodium benzoate (5 mg) were dissolved in deionised water while stirring at 700 rpm. Subsequently, the compounds in DMSO were incorporated into the mixture. The mixture was stirred for 30 minutes at 700 rpm and neutralised with 0.5%

triethanolamine until a gel formed. Visual inspection evaluated the colour, homogeneity, consistency, and phase separation. The pH value was measured using a digital pH meter, and the viscosity was assessed with a viscometer (Atago, Japan). The concentration of AmB was determined as previously described.

Mice, Ethical Commitment

BALB/c mice (8–10 weeks of age) were obtained from the National Institutes of Health in Bogotá, Colombia. They were maintained on a 12-hour light/dark cycle at 23°C, with 55% relative humidity, and provided with access to food and water *ad libitum*. Animal welfare was prioritised throughout the study. Animal procedures were performed strictly in accordance with the recommendations in the NIH Guide for the Care and Use of Laboratory Animals, published by the National Research Council (US) Committee in 2011. The Ethics Committee of the Industrial University of Santander, Bucaramanga, Colombia (CIENCI, Code 4110) approved the protocols used. Mice were monitored for behavioural changes and signs of stress. At the end of the experiments, they were anaesthetised with a combination of ketamine and xylazine and euthanised by cervical dislocation.

Irritation Test

Healthy BALB/c mice (n = 2) were topically treated with 50 µL of 1% ZIF-8, 0.5% AmB, or 0.5% ZIF-8@AmB hydrogel over the shaved area for 4 hours. Signs of swelling or redness at the application site were observed at multiple time points and scored from 0 (no irritation) to 4 (severe irritation).[29]

Antileishmanial Activity

Mice were infected subcutaneously on the shaven rump above the tail with 5×10^5 stationary-phase *L. amazonensis* (MHOM/BR/73/LV78) promastigotes suspended in 100 µL of PBS at pH 7.2. When the lesion size (LS) ranged from 20 to 30 mm², the mice were randomly divided into three groups (n = 5 per group) for treatment with 1% ZIF-8, 0.5% AmB, and 0.5% AmB@ZIF-8 hydrogels. For treatment, 100 µL of the gel was applied to the CL lesion, and after 15 minutes (to allow for gel absorption), the mice were returned to their respective cages. The mice received treatment once daily for 30 days. Lesion sizes (LS) were measured using a digital calliper (Jencons Scientific Ltd., UK). The area (mm²) was calculated using the formula of an ellipse: Area = $\pi \times r_1 \times r_2$, where r_1 denotes the longitudinal radius and r_2 the transverse radius. Lesion sizes were assessed at various time points, including 0, during treatment, and 30 days post-treatment. The animals were euthanised 30 days after treatment. A photographic register was performed. The LS reduction percentage was calculated as follows (LS0 - LSx) / LS0 ×100, where LS0 = Initial lesion size and LSx = lesion size at each evaluation day. The amastigote burden was determined microscopically in skin smears stained with Giemsa, using a semi-quantitative method to indicate the presence or absence of intra- and extracellular amastigotes: (0) absence, (+) scarce, (++) moderate, and (+++) abundant. Body weight and signs of pain, suffering, and skin irritation were recorded weekly.

Statistical Analysis

Results of in vivo antileishmanial activity from each experimental group were expressed as the mean lesion area (mm²) ± standard deviation. One-way ANOVA and Tukey's multiple comparison tests were used to statistically analyse the evolution of lesion size within each group. Other comparisons were performed using the Student's *t*-test. Statistical analysis was performed using GraphPad Prism® (Version 8.0; GraphPad Software, San Diego, CA). Statistical significance was considered at a p-value of less than 0.05.

Results and Discussion

Chosen Drug: AmB

The antileishmanial drugs used are shown in Table S1. The drugs have different structures and, except for MTF, do not adhere to rule 5. This guideline is utilised to predict the permeability of drugs through the skin.[30] The most potent drugs against *L. amazonensis* promastigotes were AmB, PMD, and KTZ, with IC_{50} values ranging from 0.3 to 2.8 µg/mL, followed by MTF with IC_{50} values ranging from 5.8 to 7.9 µg/mL, and PAR and Sb^{III} with IC_{50} values ranging from 29.6 to 34.1 µg/mL (Table S3). Additionally, quercetin (a plant-derived flavonoid) and curcumin (a diferuloylmethane from *Curcuma longa*) were selected based on their physicochemical properties, compliance with Rule 5, and previously reported activities against certain species of

Leishmania.[31–33] The potency of quercetin against promastigotes was low, while curcumin displayed higher potency with an IC_{50} of 7.9 µg/mL. However, curcumin showed a low selective index (Table S4).

We chose AmB, which showed high potency and selectivity (SI 33.2). AmB is a polyene macrolide antibiotic that binds to ergosterol in the parasite membrane, creating hydrophilic pores, disrupting membrane integrity, and causing cell death.[34] Liposomal (L-AmB) is administered by infusion at 2–3 mg/kg/day, up to a total dose of 20–60 mg/kg, for cases of mucosal, unresponsive, and complicated American-CL.[2] Despite its suboptimal physicochemical properties for transdermal use, self-aggregation, toxicities, and high cost, the topical application of AmB shows promise for further reformulation studies due to its excellent antileishmanial profile in experimental models and humans.[3,34,35] Various topical DDS have been developed to enhance AmB dermal penetration and antileishmanial efficacy.[7,10–12]

MOF Preliminary Studies

Commercially Available

We used two commercial MOFs: Fe-BTC and ZIF-8 (Table S2). Iron and zinc are essential metals in eukaryotes and play a crucial role in the human body. Fe-BTC has the same chemical composition as the synthetic MIL-100(Fe), a well-studied DDS material.[17] Some differences include the lack of a defined crystalline structure and variances in catalytic or oxidative functions.[36] Structurally, commercial ZIF-8 is similar to laboratory-prepared MOFs, with some differences partly due to the final particle size.[37] ZIF-8, also known as the zeolitic imidazolate framework, contains an imidazole group and a histidine amino acid side chain. Imidazole-based drugs have been widely used in various clinical conditions, including leishmaniasis (see ketoconazole, Table S1).[38] ZIF-8 has been extensively studied in the medical field due to its low toxicity, excellent biocompatibility, easy surface functionalisation, efficient drug loading, slow-release properties, and biodegradability under acidic conditions.[39,40] This last characteristic caught our attention. *Leishmania* is an intracellular parasite that can survive and multiply effectively in the cytoplasmic phagosome, an organelle characterised by a very low pH.[41]

Dispersion and Particle Sizes of MOFs Without Drug

After 24 hours of exposure to the tested solvents, ZIF-8 exhibited partial dissolution in 1% Tween 80 (pH 5.5–7.2) and triacetin (pH 5–6), which are a nonionic surfactant and glyceryl triacetate, respectively, commonly used as pharmaceutical excipients. Complete and intermediate solubility of ZIF-8 was observed in acidified 10% Tween 80 within the pH ranges of 2.40–5.03 and 5.73–6.02, respectively. In contrast, the Fe-BTC samples exhibited no changes at the tested pH levels.

In the final experiment, Fe-BTC and ZIF-8 suspended in DMSO, ethanol, and Type I water appeared homogeneous after sonication; however, all samples precipitated following centrifugation (Table S5). Notably, the solution of ZIF-8 in acidified DMSO remained transparent and showed no precipitation after centrifugation, similar to the behaviour observed in other acidified solvents at pH levels below 5.0. The particle size values of MOFs in solution ranged in the micrometre scale and showed moderate to high levels of aggregation (Table S5). For ZIF-8 in DMSO, ethanol, and Type I water, the sizes were 2.5 ± 0.4 µm, 1.2 ± 0.16 µm, and 2.9 ± 0.48 µm, with a PDI of 0.117, 0.651, and 0.298, respectively (Table S5). The ZIF-8 sample exhibited a more significant variation in size in ethanol, although the overall particle size was smaller (Table S5). The method of synthesis affects the particle size of ZIF-8. For example, using sonochemical or dry-gel conversion methods yields smaller particle sizes (300−500 nm) compared to solvothermal methods (150−200 nm) or commercial ZIF-8 (0.5−20 µm).[42] The particle size of ZIF-8 in acidic DMSO was 11.13 ± 0.01 nm with a PDI of 0.117 (Table S5), indicating its disintegration under low pH conditions.[43] The particle size of Fe-BTC was 0.59 ± 0.09 µm with a PDI of 0.231 (Table S5 and Figure 1A).

THP-1 Cells and MOFs

The MOF treatment showed low toxicity in THP-1 cells after 72 h of incubation, with CC_{50} values ranging from 114 to 151 µg/mL (Table S4). Various cell lines, incubation times, and MOF particle sizes were utilised for cell toxicity experiments. For instance, despite being approximately ten times smaller (200 nm), nano ZIF-8 was nearly six times more toxic than the commercial ZIF-8 used in our study.[44] Among Fe-based MOFs, nanoMIL-88A (150 nm) on mouse macrophages exhibited a CC_{50} value of 57 ± 11 µg/mL, whereas MIL-53 (2.5–3.0 µm) on HepG2 cells showed a CC_{50} value of greater than 100 µg/mL.[17,45] No cell toxicities (CC_{50} > 1000 µg/mL) were induced by a panel of Fe, Zr, and Al-

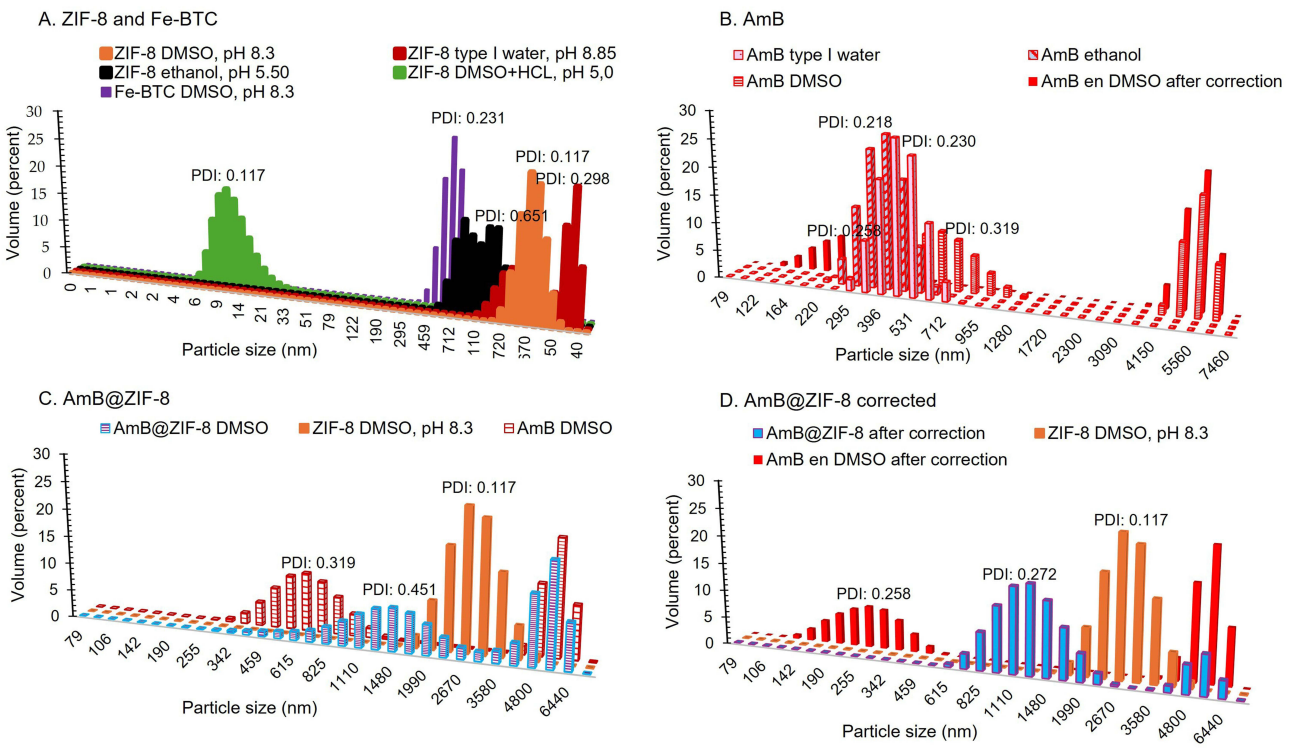

Figure 1 Particle size distribution and polydispersity index (PDI) of the samples. The size and PDI were determined using dynamic light scattering measurements. ZIF-8, Fe-BTC (**A**), and AmB (**B**) were dispersed in DMSO, ethanol, or Type I water. Additionally, ZIF-8 was diluted in acidified DMSO (**A**). The AmB@ZIF-8 conjugate was dispersed in DMSO (**C** and **D**). All samples were sonicated with an ultrasound tip for 1 minute (**A**–**C**) or 3 minutes (**D**) before measurements were taken.

based MOFs on human dermal fibroblasts, 3T3, and Hela cells after a 4-h incubation.[46] In our study, adherent THP-1 cells remained healthy after exposure to Fe-BTC (60 µg/mL) for 24 hours (Figure S1). Some cells exhibited a vacuolated cytoplasm with black granular material inside, possibly due to ferrous deposits. When treated with ZIF-8 at a similar concentration, some cells lost adherence and decreased in size, and at 25 µg/mL, some vacuoles were observed inside the cells (Figure S1). Although we could not demonstrate any specific cell uptake mechanism in this initial experiment, some changes occurred at the cytoplasmic level, indicating MOF cell endocytosis.

AmB-Loaded-ZIF-8 (DLC% and EE% Analysis)

Our study consisted of six experimental replicates with an initial AmB: ZIF-8 ratio of 1.5:1.0. We achieved a DLC ± SD of 59.6% ± 3.86 (loading capacity of 0.596 g/g). Our DLC value was higher than that of some DDS-AmB formulations, which had DLC levels below 20 wt%, but was similar to the value obtained by Chen et al[28] using a similar protocol. ZIF-8 has been impregnated with various drugs, including doxorubicin and 5-fluorouracil, displaying DLC values ranging from 0.049 g/g to 0.660 g/g at different drug-to-MOF ratios (1:6.66, 1:0.33, and 1:0.66).[18,47,48] Differences in DLC may be related to the molecular weight and charge of the cargo, particle size, and the drug-to-MOF ratio used. In MIL-100, −101 and −53, differences in ibuprofen DLC (0.19−0.35 g/g) could be related to surface area or pore volume.[49] It has been suggested that a disadvantage of nano-ZIF-8 as a DDS could be its small pore size compared to other mesoporous nanoparticles, such as SiO2, ZnO, and Fe3O4.[39] After using the Nanosep Centrifugal Device, most of the AmB was filtered into the external phase, resulting in a low EE of 6.67%. This is significantly lower than other lipid-based DDS for AmB, which typically have EE ranging from 50% to 99%.[50] The EE% of MOFs may be influenced by various factors, including the type of MOF and drug used, as well as the MOF-drug loading methodology. Among the two drug-loading techniques used, the two-step or post-synthesis method (ie impregnation technique) can result in low loadings and either rapid or slow in vitro release (IVR) of the drug.[51] For instance, doxorubicin (DOX; MW: 543.5, log P: 1.27) was incorporated into commercial ZIF-8, exhibiting an IVR of 66% after 30 days.[52] and gentamicin (GEN, MW 477.6, log

P −3) to nano-ZIF-8 resulted in a DLC of 19%, a particle size of 200 nm, and an IVR at pH 5.0 higher than at pH 7.4 (84% at 80 hours).[53] Employing a one-step methodology (MOF and drug integrated during synthesis) as a one-pot approach, Zheng et al synthesised DOX@ZIF-8 particles that exhibited an EE of 20%, a particle size of 50 nm, and efficient, pH-dependent drug delivery for cancer therapy.[51] A one-step methodology was also employed for loading curcumin into ZIF-8 as a drug carrier, demonstrating an EE of 83.3%, chemical stability, pH-dependent release, a particle size of 145 nm, and change from colorless to orange.[54] In our case, using a high amount of AmB may have allowed commercial ZIF-8 to absorb the maximum possible quantity of AmB into its structure. However, after centrifugation, a significant portion of the AmB in the pellet may not be confined within the ZIF-8 pores, as indicated by the high DLC (59.6%) and low EE (6.7%) achieved. In a system of AmB-polymeric micelles (~80 nm, PDI < 0.2, EE 95%, DLC 20%), the DLC and EE were found to be related to the polymer concentration; an increase in polymer content resulted in a decrease in the DLC percentage, whereas the EE percentage increased.[55] We suggest exploring different AmB: ZIF-8 ratios (up to 1:4) in future work, along with minimising the particle size in the solution, as we will explain later.

Particle Sizes of AmB and AmB@ZIF-8

For AmB, the mean particle size ± SD in DMSO, ethanol, and Type I water after sonication was 608.0 ± 10.8 nm, 505.2 ± 3.2 nm, and 453.9 ± 3.2 nm, respectively. The PDIs were 0.319, 0.239, and 0.230. Since the limit of PDI for monodispersed particles is less than 0.2, it can be concluded that AmB showed moderate aggregation (oligomerisation) in all solvents. AmB is a large, amphoteric molecule (Table S1) that is soluble in DMSO (30–40 mg/mL) but not in water (0.08 mg/mL).[33] It has been formulated with sodium deoxycholate (Fungizone) or in a lipid formulation, such as Ambisome (L-AmB), to allow higher doses and reduce aggregation and nephrotoxicity.[56] Due to its complex chemical structure, AmB can self-assemble into monomers, oligomers, and polyaggregates in aqueous media.[57] In our work, the aggregation of AmB in solution correlates with particle size heterogeneity (Figure 1B and D). Smaller particle sizes were demonstrated by Fungizone and L-AmB (~100 nm), but higher values of Fungizone in NaCl at pH 7.2 have also been displayed (3310 nm, PDI 0.398).[58] In DMSO, the particle size of AmB@ZIF-8 was 1370 ± 2.6 nm (PDI: 0.45, polydisperse), which is almost twice as low as that of ZIF-8 (2537 nm, PDI: 0.117, monodisperse) and higher than that of AmB (Figure 1A and C). After correction, the AmB@ZIF-8 size was similar but more homogeneous (1458 ± 0.16 nm, PDI: 0.272). For AmB, the mean size was reduced to 248.3 ± 10.1 nm, but the PDI remained similar (PDI: 0.228) (Figure 1D). As previously described, the particle size and PDI of commercial ZIF-8 ranged from 1200 to 2900 nm and 0.1 to 0.6, respectively, depending on the solvent used. The observed decrease in particle size following acidification was attributed to the degradation of ZIF-8 (11 nm, PDI 0.1), confirming its breakdown in acidic environments (pH < 6) and its stability in neutral and alkaline conditions (pH ~7.4) (Table S5). Many investigators have used the terms "nanoparticles" and "microparticles" interchangeably; however, compared to larger particles, nanoparticles with a diameter of 200 nm or less are more efficient in penetrating biological barriers for targeted drug delivery. In some cases, microparticles (1–5 μm) can elicit lasting immune responses, making them suitable for vaccine delivery. Additionally, hydrophobic microparticles, such as polycaprolactone and polylactic acid, can serve as intriguing drug carriers or scaffold components in pharmaceuticals and tissue engineering.[59,60] However, this will not apply here, as topical DDS is generally sized in the nm range. Due to the significant impact of the synthesis method and conditions- such as solvent choice, pH, and temperature- on the structural and chemical properties of pure ZIF-8, including its particle size, appropriate methodologies for AmB@ZIF-8 conjugation, whether using a one-step or two-step method, must be employed to achieve smaller particle sizes than those obtained in our work.

Cumulative Release (%) of AmB From ZIF-8

Various methodologies have been developed to evaluate the AmB IVR from their DDS at different stages of product development; however, no standardised IVR assay is currently available. In our case, during this initial phase, we utilised DMSO solutions of AmB@ZIF-8 and AmB-free in dialysis tubing (3500 Da pores) along with a receptor solution that permitted AmB solubility (80% PBS at pH 7.4, 10% Tween 20, and 10% DMSO), at 25 °C and 150 rpm stirring for 96 hours. In both AmB-free and conjugated samples, the release percentage of AmB remained below 2%. (Figure 2). After 24 hours, the release of AmB became slower. The rate of AmB release from AmB@ZIF-8 was lower than that of free AmB (0.73% vs 2.3%) ($p < 0.05$) (Figure 2). This could suggest that ZIF-8 as a DDS could retain AmB release for

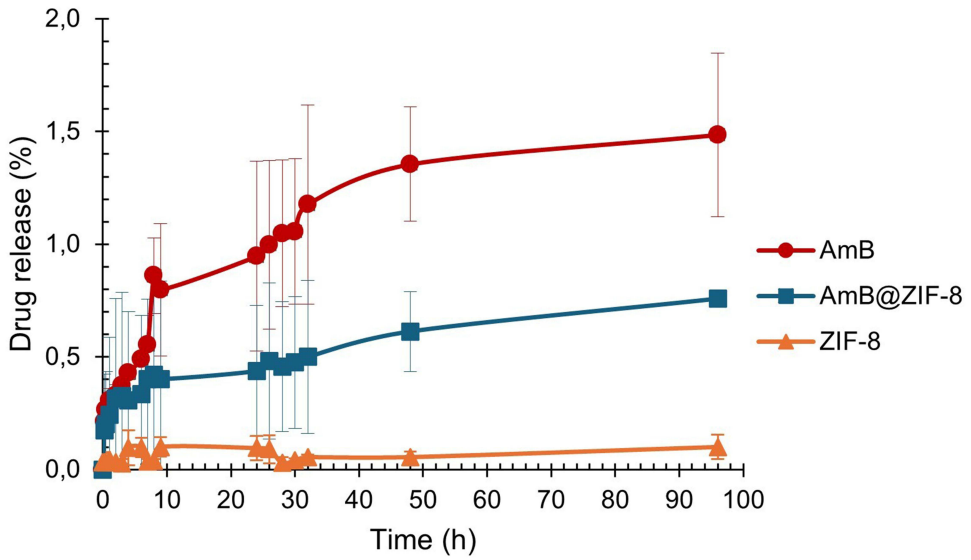

Figure 2 In vitro cumulative drug release (%) of AmB. The release profile of AmB over time from free and conjugated AmB (AmB@ZIF-8) was assessed using dialysis bags. The receptor solution consisted of PBS, Tween 20, and DMSO, while ZIF-8 alone served as the control.

a longer duration than the unloaded drugs. Several parameters may affect the low AmB release percentages, including the amount of drug incorporated, the ZIF-8 structure, acid degradation, and AmB characteristics, including AmB aggregation.[48,61,62] Additionally, certain factors related to the testing conditions, such as membrane pore size, receptor medium, temperature, and pH, may also play a role. The degree of AmB aggregation and the process of DDS preparation influence the release rate.[34] In our case, as we described earlier, AmB formed oligomers in DMSO, and perhaps they cannot escape from a 3500 Da membrane. The amphoteric nature and structure of AmB, characterised by a hydrophobic polyene hydrocarbon chain and a hydrophilic polyhydroxy chain domain, present significant challenges. The aggregation state of AmB affects its toxicity and release rate. Different solvents used exhibited various aggregation states of AmB, such as γ-cyclodextrin (γ-CD), which maintains monomeric AmB, and bile salt deoxycholate (Fungizone), which forms micelles.[63] Mixtures of them with PBS, organic solvents, or DMSO have been used for the IVR test, displaying cumulative AmB drug release of more than 70% within 24 hours.[12,63,64] We used a solution receptor where the AmB was soluble; however, most studies utilise at least 10 kDa cellulose membranes, which may be one important reason for the low AmB release obtained in our study. Recently, an IVR assay using a standardised dissolution apparatus flow-through cell (USP 4) under sink conditions (AmB 10 µg/mL), with a release medium containing 5% γ-CD and a pH of 7.4, at 55 °C, was proposed as a useful tool for characterising the drug release profiles of different liposomal AmB formulations.[65] A well-standardised IVR assay in AmB-DDS discovery is essential for developing new DDS that maintain the high efficacy of AmB while minimising the risk of AmB-free toxicity.

Characterisation

UV-Vis Spectra of ZIF-8@AmB and Their Components

ZIF-8 absorbs UV light at 210–216 nm in ultrapure water and 258–267 nm in DMSO (Figure 3A). Previous studies have also found that ZIF-8 absorbs UV light in the range of 210 to 250 nm (230 nm) due to the absorbance of its organic ligand, 2-methylimidazole.[66] The absorption of ZIF-8 in the UV region makes it a promising candidate for sunscreen protectors or topical skin treatments. The aggregated form is thought to be more toxic and, in some cases, less active than the monomeric form. It is also considered that monomeric forms cannot pass through a lipid membrane. The AmB@ZIF-8 absorption spectrum in both experimental replicates showed four bands typical of the monomeric form of AmB (Figure 3B). These bands remained present after 30 days from preparation (Figure 3B). Furthermore, a band at 256 nm indicates the presence of the imidazole group in the AmB@ZIF-8 conjugate, confirming the incorporation of ZIF-8 into

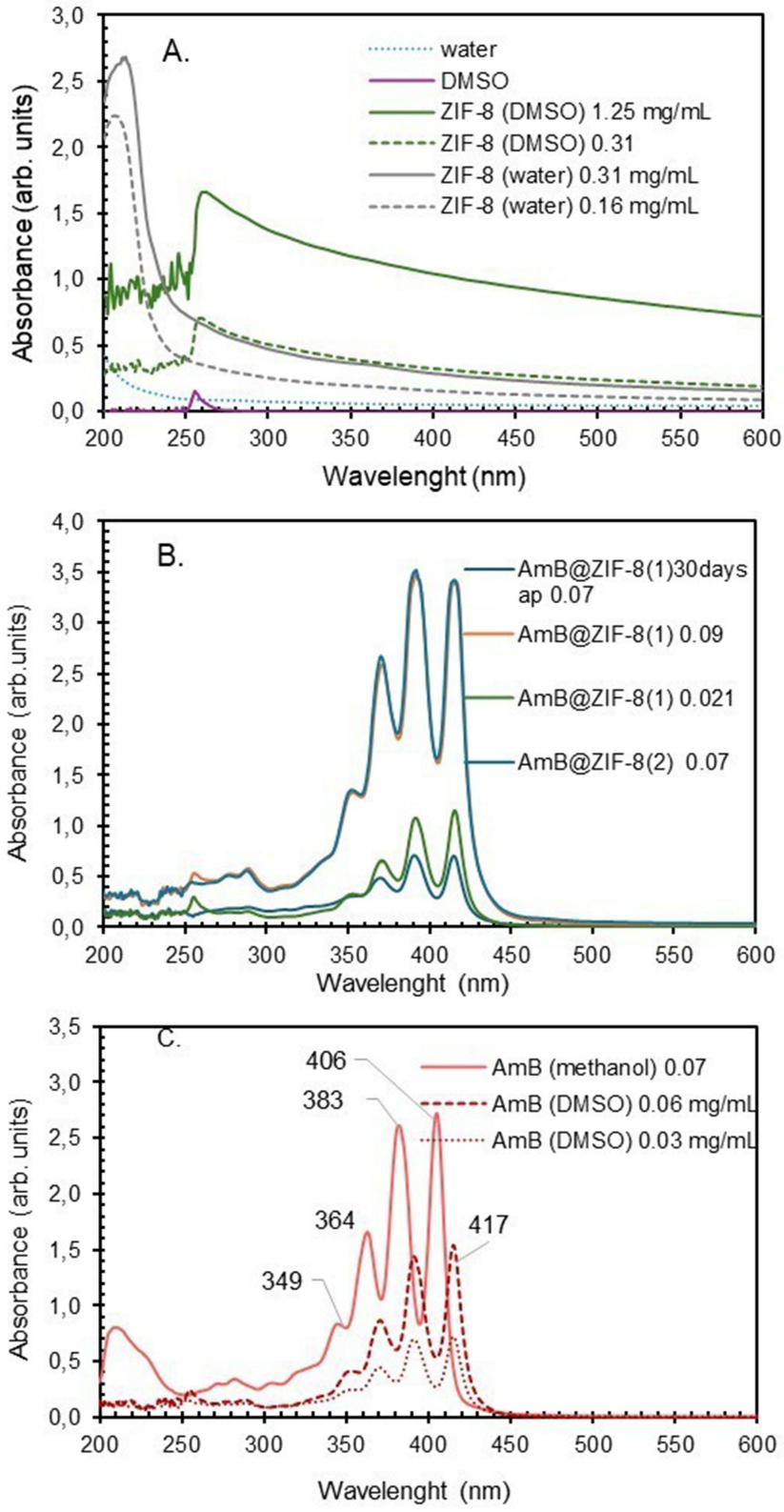

Figure 3 UV spectroscopy characterisation. The figure presents the UV-Vis spectra of ZIF-8 in DMSO and water (**A**) and the spectra of AmB@ZIF-8 in DMSO (**B**). (**B**) includes data from two experiments, labelled as 1 and 2, along with the spectra of AmB@ZIF-8 taken 30 days after preparation, which is designated as "ap". (**C**) displays the UV-Vis spectra of two concentrations of AmB dissolved in DMSO and one concentration in methanol.

https://doi.org/10.2147/JEP.S511808

the conjugate. On the other hand, the spectrum of AmB depends on its aggregation state due to its amphiphilic structure. In an aqueous solution, AmB is aggregated and displays a peak at 328 nm. However, in organic solvents such as methanol or DMSO, AmB is a monomer and exhibits four peaks at 349, 394, 383, and 406 nm (Figure 3C).

FTIR Spectroscopy

As shown in Figure 4A, the commercial ZIF-8 displays peaks at 3136, 1586, 1425, 1310, 1146, 996, 759, 694, and 420 cm^{-1}, which are consistent with those previously documented by Zang et al in 2018.[67] The peak at 3136 cm^{-1} corresponds to the asymmetric stretching vibration mode of the aromatic C-H bond, and the peaks at 2926 and 1586 cm^{-1} are observed as the stretching vibration of the H-C–N bond in 2-methylimidazole and the stretching vibration mode of the C-N bond, respectively. Signals between 1300–1460 cm^{-1} for the entire ring stretching. The band at 1146 cm-1

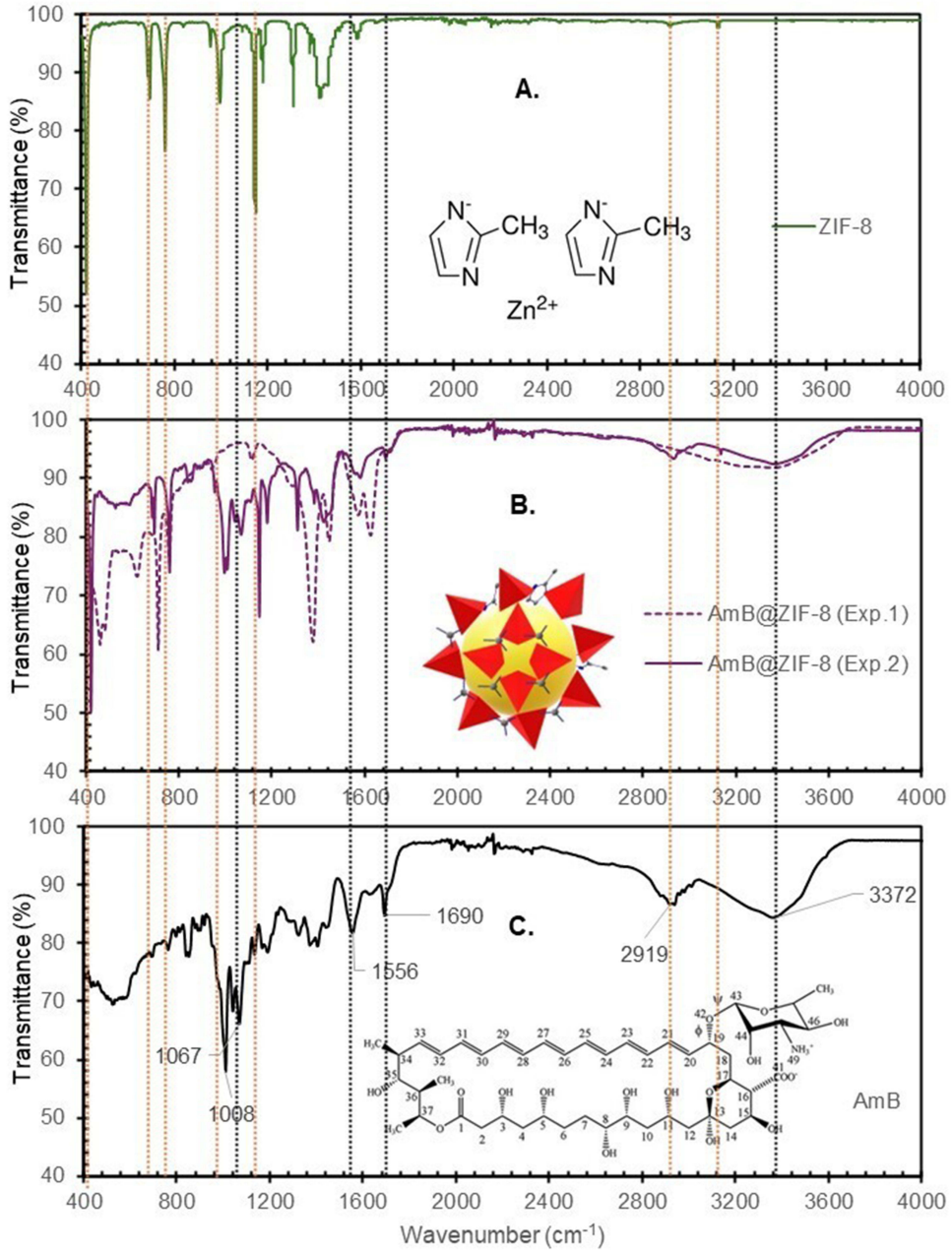

Figure 4 FTIR spectroscopy. The figure shows the FTIR spectra of ZIF-8 (**A**), AmB-8@ZIF-8 (**B**), and AmB (**C**). The Orange and black dashed lines indicate the characteristic peaks of ZIF-8 and AmB, respectively. The structures of each component (or icon) are included.

originates from aromatic C-N stretching, while the peaks at 996 cm^{-1} and 760 cm^{-1} correspond to C-N and C-H stretching, respectively. The out-of-plane bending vibration of the aromatic H was observed at 694 cm^{-1}. The Zn-N stretching band was observed at 426 cm^{-1} (420 nm^{-1} in our case), indicating that zinc ions chemically combined with the nitrogen atoms of the methylimidazole groups to form the imidazolate.[67] The FTIR spectrum of the AmB molecule exhibited vibrational modes corresponding to its functional groups, including −COO-, −NH3+, −OH, and C−C bonds. We observed stretching vibrational modes between 3300 and 3500 cm^{-1} due to O−H and N−H bonds. In the spectral region between 1500 and 1800 cm−1, we observed the stretching vibrations of C=C, C=O and C-NH_3 groups. Specifically, vibrational modes of C=C, C=O and C-NH_3 bond appear at 1690, 1556 and 1050 cm^{-1} (Figure 4C). The FTIR spectrum of ZIF-8@AmB exhibits characteristic peaks of both ZIF-8 and AmB; however, the peaks at 1690 and 1556 cm-1 of AmB show a slight shift, likely due to the interaction between AmB and ZIF-8 (Figure 4B).

Fesem

Figure S2A and B show the microscopic morphology of the AmB@ZIF-8 complex and commercial ZIF-8, respectively. The SEM micrograph of AmB@ZIF-8 MOF (Figure S2A) shows hexagonal shape micro and nanoparticles (~400 nm) aggregates. The SEM micrograph (Figure S2B) indicates that ZIF-8 MOF has a non-well-defined morphology. It is observed aggregated of asymmetrical morphology nanoparticles (~400 nm). Finally, EDS analysis corroborated the presence of the ZIF-8 MOFs in the AmB@ZIF-8 complex.

Antileishmanial Activity of AmB@ZIF-8 (in vitro)

The treatment with AmB@ZIF-8 against *L. amazonensis* promastigotes demonstrated a dose-response effect. There were no significant differences in the antileishmanial activities of AmB@ZIF-8 and free AmB, as indicated in Figure 5A. The IC_{50} values for both compounds were 0.4 to 0.8 µg/mL (Table S4). In contrast, treatment with ZIF-8 alone showed very low antileishmanial activity (Figure 5A). The experiment confirmed that AmB potency against parasites remained stable after using the described impregnation method.

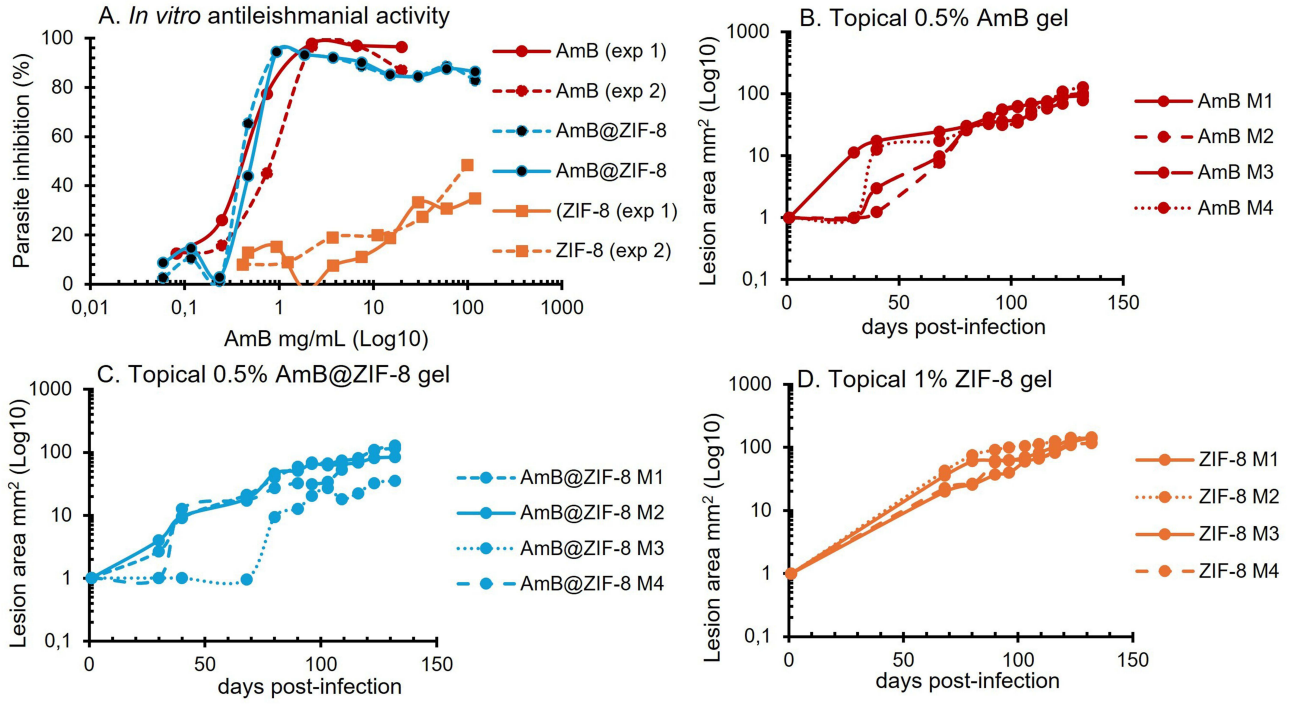

Figure 5 In vitro and in vivo activities of AmB@ZIF-8, AmB and ZIF-8. Dose-response activities of the compounds against *L. amazonensis* promastigotes (**A**). Evolution of lesion size (mm^2) in BALB/c mice with cutaneous leishmaniasis caused by *L. amazonensis* after topical treatment with AmB (**B**), AmB@ZIF-8 (**C**), and ZIF-8 (**D**) for 30 days. The figure displays the results observed in each mouse (M).

https://doi.org/10.2147/JEP.S511808

In vivo Experiments

Hydrogels for in vivo Studies

The characteristics of each formulation are summarised in Table S3. They were easy to prepare, homogeneous, and without lumps. The pH values of AmB and AmB@ZIF-8 gels were neutral, at 6.7 and 7.1, respectively. Their intrinsic viscosities were 3811 and 4609 cP, respectively. Since the skin pH is acidic (pH ~5), slightly acidic topical formulations are designed to maintain stratum corneum homeostasis and barrier permeability.[68] Our prepared gels were neutral or basic, with a pH range of 6.69 to 8.7. As ZIF-8 is a pH-sensitive molecule, the ZIF-8 topical formulation must be designed to prevent disintegration before use. Consequently, we did not acidify any of our tested topical formulations for our purpose.

Antileishmania Activity of Topical Treatments in Infected BALB/c Mice

The progression of lesions in BALB/c mice infected with *L. amazonensis* and treated with AmB, AmB@ZIF-8, and ZIF-8 hydrogels are shown in Figure 5B–D). Topical treatment with AmB@ZIF-8 was unable to cure *L. amazonensis*-CL (Figure 5C and Figure S3). Both AmB and AmB@ZIF-8 hydrogel treatments initially attempted to stabilise the lesion size; however, the lesions considerably increased in the end. Cutaneous lesions in the ZIF-8 group continued to enlarge. Although an attempt was made to close the ulcers (open lesions) after treatment, a few changes were observed in the nodule (Figure S3). No significant differences were noted between the groups ($p > 0.05$). We decided to euthanise the mice after 30 days to prevent their suffering. Initially, the lesions appeared as papules and progressed into raised nodules with red ulcers and, in some cases, a necrotic background (Figure S3). At the end of the experiment, the lesions exhibited a high burden of amastigotes.

The intravenous administration of AmB is commonly used, while the topical application of AmB is still under research. Initially, it was observed that AmB has unfavourable physicochemical characteristics for topical administration (Table S1), including a high molecular weight, amphoteric nature, tendency to self-aggregate, and low aqueous solubility at physiological pH. A 3% AmB (Anfoleish®) cream was tested on Colombian CL patients. It was found to be safe, but it showed a low cure rate of ~39.4%.[4] The lack of AmB in the plasma indicated low permeability through the skin. Various strategies have been employed to enhance drug-dermal penetration. In 2011, a clinical trial in Iranian CL patients used a topical liposomal (L)-AmB solution, resulting in a 56.4% efficacy comparable to intralesional Sb^V.[69] Treatment with different AmB-DDS, such as niosomes, liposomes, and transferosomes, has been used topically in BALB/c mice with CL by *L. major* or *L. amazonensis* yielding some results regarding the reduction of lesion size or parasite loads.[70] Although the initial lesion sizes were lower than those predicted by our model, a complete cure was not achieved at the end of the experiment. The efficacy of nano-L-AmB 0.4% (administered twice daily for four weeks) was demonstrated in mice infected with *L. major*.[71] The same formulation and dose were found to be safe in Iranian CL-infected patients, and 19 out of 20 patients achieved a complete cure.[7] This result motivates modifications in our AmB@ZIF-8 regarding the drug: MOF ratio and particle size, which may enhance in vivo efficacy.

Despite our negative results, we are convinced that ZIF-8 or MOFs, in general, may offer advantages over other lipid-based DDS for AmB delivery. Its high surface area and tunable porous structure, combined with the biocompatibility of metal (zinc) and organic linker, as well as the loading capacity of lipophilic and hydrophilic compounds with varying molecular weights, are remarkable.[14,18,20,72] Interestingly, this functionality enables the controlled release of medication in response to pH, light, and temperature, as is the case in the environment of skin diseases (such as cancer, wounds, and chronic lesions), facilitating targeted therapy while minimising side effects.[72–74] Recently, biomolecule-engineered metal-organic frameworks (Bio-MOFs) have been developed by integrating biomolecules into MOFs, showcasing unique catalytic and biological properties. Some interesting examples using ZIF-8 include a nanocomposite of ZIF-8 and polyglutamic acid (ZIF-PGA), which incorporates ciprofloxacin and methylene blue as a photosensitizer (ZIF/PGA-C/M), and a ZIF-8-loaded hydrogel with curcumin combined with a methylcellulose/carboxymethyl chitosan temperature-sensitive hydrogel. Both systems demonstrated controlled drug release under various conditions (pH, temperature, and presence of enzymes) and exhibited increased biological activity in vitro and in vivo compared to the control groups.[73,74]

Skin Irritation Assessment

In this study, none of the mice showed signs of irritation or skin oedema at the site of hydrogel application 14 days after treatment. (Figure S4).

Conclusion

Considering the commercial availability and instability of ZIF-8 at acidic pH- proposed for endosomal delivery- and the superior potency of AmB against *L. amazonensis* promastigotes, ZIF-8 was suggested as a topical DDS for AmB in experimental CL. The conjugation of AmB to ZIF-8 was demonstrated. However, there were very low EE% and AmB IVR (6% and 2%). No differences were observed in the in vitro activity of AmB and AmB@ZIF-8 against promastigotes, indicating that AmB retains its efficacy when incorporated into ZIF-8. Hydrogels containing 1% ZIF-8, 0.5% AmB, or 0.5% conjugates were easily prepared and suitable for dermatological use. However, topical treatment was ineffective in healing mice with CL lesions. Several reasons may explain these negative results, including the large size of the commercial ZIF-8, AmB aggregation in solution, the excess of AmB used for impregnation (AmB: ZIF-8 ratio of 1.5:1.0), and the IVR assay conditions. Smaller particle sizes (~ 200 nm) can be achieved using synthesis methodologies such as one-pot synthesis; AmB aggregation could be avoided under sink conditions or curing approaches; AmB@ZIF-8 synthesis could be performed using an AmB: ZIF ratio of 1:4; and IVR assays could be standardised with a different cellulose membrane pore size, slight acidic pHs, higher temperatures, and reagents that allowed monomeric AmB. It is suggested that ZIF-8 could be used with other drugs, such as miltefosine or pentamidine, which have shown topical activity in some experimental studies with American CL species.

Acknowledgments

We thank the Vicerectoria de Investigación y Extensión de la Universidad Industrial de Santander, grant number 3740, and Professor Rafael Cabanzo Hernández and Yuly Prada Vargas, from the Industrial University of Santander, Bucaramanga, Colombia, for their help with some characterisation procedures. We sincerely thank Professor Hugo A. Estupiñán from the National University of Colombia, Medellín Campus, for supporting the SEM procedure analysis.

Disclosure

The authors report no conflicts of interest in this work.

References

1. de Vries HJC, Schallig HD. Cutaneous Leishmaniasis: a 2022 Updated Narrative Review into Diagnosis and Management Developments. *Am J Clin Dermatol*. 2022;23(6):823–840. doi:10.1007/s40257-022-00726-8
2. Burza S, Croft SL, Boelaert M. Leishmaniasis. *Lancet*. 2018;392(10151):951–970. doi:10.1016/S0140-6736(18)31204-2
3. Pan American Health Organization. *Manual of Procedures for Leishmaniasis Surveillance and Control in the Region of the Americas*. 2nd edition. PAHO; 2024. https://iris.paho.org/handle/10665.2/59237. Accessed August 6, 2024.
4. López L, Vélez I, Asela C, et al. A Phase II study to evaluate the safety and efficacy of topical 3% amphotericin B cream (Anfoleish) for the treatment of uncomplicated cutaneous leishmaniasis in Colombia. *PLoS Negl Trop Dis*. 2018;12(7):e0006653. doi:10.1371/journal.pntd.0006653
5. Soto J, Paz D, Rivero D, et al. Intralesional pentamidine: a novel therapy for single lesions of Bolivian cutaneous leishmaniasis. *Am J Trop Med Hyg*. 2016;94(4):852–856. doi:10.4269/ajtmh.15-0640
6. Neira LF, Mantilla JC, Escobar P. Monitoring cutaneous leishmaniasis lesions in mice undergoing topical miltefosine treatment. *Sci Pharm*. 2023;91(4):54. doi:10.3390/scipharm91040054
7. Khamesipour A, Mohammadi A, Jaafari M, et al. Pilot study of safety and efficacy of topical liposomal amphotericin B for cutaneous leishmaniasis caused by Leishmania major in Islamic Republic of Iran. *EMHJ*. 2022;28(9):658–663. doi:10.26719/emhj.22.070
8. Carneiro G, Aguiar MG, Fernandes AP, Ferreira LAM. Drug delivery systems for the topical treatment of cutaneous leishmaniasis. *Expert Opin Drug Deliv*. 2012;9(9):1083–1097. doi:10.1517/17425247.2012.701204
9. de Souza A, Marins DSS, Mathias SL, et al. Promising nanotherapy in treating leishmaniasis. *Int J Pharm*. 2018;547(1–2):421–431. doi:10.1016/j.ijpharm.2018.06.018
10. Butani D, Yewale C, Misra A. Amphotericin B topical microemulsion: formulation, characterization and evaluation. *Colloids Surf B Biointerfaces*. 2014;116:351–358. doi:10.1016/j.colsurfb.2014.01.014
11. Dar MJ, Khalid S, McElroy CA, Satoskar AR, Khan GM. Topical treatment of cutaneous leishmaniasis with novel amphotericin B-miltefosine co-incorporated second generation ultra-deformable liposomes. *Int J Pharm*. 2020;573:118900. doi:10.1016/j.ijpharm.2019.118900
12. Riaz A, Hendricks S, Elbrink K, et al. Preparation and Characterization of Nanostructured Lipid Carriers for Improved Topical Drug Delivery: evaluation in Cutaneous Leishmaniasis and Vaginal Candidiasis Animal Models. *AAPS Pharm Sci Tech*. 2020;21(5):275. doi:10.1208/s12249-020-01819-5

13. Carvalheiro M, Vieira J, Faria-Silva C, Marto J, Simões S. Amphotericin B-loaded deformable lipid vesicles for topical treatment of cutaneous leishmaniasis skin lesions. *Drug Deliv Transl Res*. 2021;11(2):717–728. doi:10.1007/s13346-021-00910-z
14. Rojas S, Colinet I, Cunha D, et al. Toward understanding drug incorporation and delivery from biocompatible metal-organic frameworks in view of cutaneous administration. *ACS Omega*. 2018;3(3):2994–3003. doi:10.1021/acsomega.8b00185
15. Taherzade SD, Rojas S, Soleimannejad J, Horcajada P. Combined cutaneous therapy using biocompatible metal-organic frameworks. *Nanomaterials*. 2020;10(12):2296. doi:10.3390/nano10122296
16. Lawson HD, Walton SP, Chan C. Metal-Organic Frameworks for Drug Delivery: a Design Perspective. *ACS Appl Mater Interfaces*. 2021;13 (6):7004–7020. doi:10.1021/acsami.1c01089
17. Horcajada P, Chalati T, Serre C, et al. Porous metal-organic-framework nanoscale carriers as a potential platform for drug delivery and imaging. *Nat Mater*. 2010;9(2):2994–3003. doi:10.1038/nmat2608
18. Sun Y, Zheng L, Yang Y, et al. Metal–Organic Framework Nanocarriers for Drug Delivery in Biomedical Applications. *Nanomicro Lett*. 2020;12 (1):103. doi:10.1007/s40820-020-00423-3
19. Fernández-Paz C, Fernández-Paz E, Salcedo-Abraira P, et al. Microencapsulated isoniazid-loaded metal–organic frameworks for pulmonary administration of antituberculosis drugs. *Molecules*. 2021;26(21):6408. doi:10.3390/molecules26216408
20. He S, Wu L, Li X, et al. Metal-organic frameworks for advanced drug delivery. *Acta Pharm Sin B*. 2021;11(8):2362–2395. doi:10.1016/j.apsb.2021.03.019
21. Zhuang J, Kuo CH, Chou LY, Liu DY, Weerapana E, Tsung CK. Optimized metal-organic-framework nanospheres for drug delivery: evaluation of small-molecule encapsulation. *ACS Nano*. 2014;8(3):2812–2819. doi:10.1021/nn406590q
22. Rojas S, Horcajada P. Understanding the incorporation and release of salicylic acid in metal-organic frameworks for topical administration. *Eur J Inorg Chem*. 2021;2021(14):1134. doi:10.1002/ejic.202001134
23. Li S, Long M, Li J, Zhang Y, Feng N, Zhang Z. Improved topical delivery of curcumin by hydrogels formed by composite carriers integrated with cyclodextrin metal-organic frameworks and cyclodextrin nanosponges. *Int J Pharm X*. 2024;8:100310. doi:10.1016/j.ijpx.2024.100310
24. Márquez AG, Hidalgo T, Lana H, et al. Biocompatible polymer-metal-organic framework composite patches for cutaneous administration of cosmetic molecules. *J Mater Chem B*. 2016;4(43):7031–7040. doi:10.1039/c6tb01652a
25. Cunha D, Ben Yahia M, Hall S, et al. Rationale of drug encapsulation and release from biocompatible porous metal-organic frameworks. *Chem Mater*. 2013;25(14):2767–2776. doi:10.1021/cm400798p
26. Ghafarifar F, Molaie S, Abazari R, Hasan ZM, Foroutan M. Fe3O4@bio-MOF nanoparticles combined with artemisinin, glucantime®, or shark cartilage extract on Iranian strain of leishmania major (MRHO/IR/75/ER): an in-vitro and in-vivo study. *Iran J Parasitol*. 2020;15(4):537–548. doi:10.18502/ijpa.v15i4.4859
27. Neira LF, Mantilla JC, Escobar P. Anti-leishmanial activity of a topical miltefosine gel in experimental models of New World cutaneous leishmaniasis. *J Antimicrob Chemother*. 2019;74(6):1634–1641. doi:10.1093/jac/dkz049
28. Chen G, Luo J, Cai M, et al. Investigation of metal-organic framework-5 (MOF-5) as an antitumor drug oridonin sustained release carrier. *Molecules*. 2019;24(18):3369. doi:10.3390/molecules24183369
29. OECD 404. Guidelines for the Testing of Chemicals. Acute Dermal Irritation/Corrosion. In: *OECD Guidelines for the Testing of Chemicals, Section 4 health Effects*. 2015.
30. Benet LZ, Hosey CM, Ursu O, Oprea TI. BDDCS, the Rule of 5 and drugability. *Adv Drug Deliv Rev*. 2016;101:89–98. doi:10.1016/j.addr.2016.05.007
31. Koide T, Nose M, Ogihara Y, Yabu Y, Ohta N. Leishmanicidal effect of curcumin in vitro. *Biol Pharm Bull*. 2002;25(1):131–133. doi:10.1248/bpb.25.131
32. Fonseca-Silva F, Inacio JDF, Canto-Cavalheiro MM, Almeida-Amaral EE. Reactive oxygen species production and mitochondrial dysfunction contribute to quercetin induced death in Leishmania amazonensis. *PLoS One*. 2011;6(2):e14666. doi:10.1371/journal.pone.0014666
33. Knox C, Wilson M, Klinger CM, et al. DrugBank 6.0: the DrugBank Knowledgebase for 2024. *Nucleic Acids Res*. 2024;52(D1):D1265–D1275. doi:10.1093/nar/gkad976
34. Frézard F, Aguiar MMG, Ferreira LAM, et al. Liposomal Amphotericin B for Treatment of Leishmaniasis: from the Identification of Critical Physicochemical Attributes to the Design of Effective Topical and Oral Formulations. *Pharmaceutics*. 2023;15(1):99. doi:10.3390/pharmaceutics15010099
35. Borges BS, De Bueno GP, Tomiotto-Pellissier F, Figueiredo FB, Soares Medeiros LC. In vitro anti-Leishmania activity of triclabendazole and its synergic effect with amphotericin B. *Front Cell Infect Microbiol*. 2023;12:1044665. doi:10.3389/fcimb.2022.1044665
36. Dhakshinamoorthy A, Alvaro M, Garcia H. Commercial metal–organic frameworks as heterogeneous catalysts. *Chem Commun*. 2012;48 (92):11275–11288. doi:10.1039/c2cc34329k
37. Nordin NAHM, Ismail AF, Mustafa A, Murali RS, Matsuura T. The impact of ZIF-8 particle size and heat treatment on CO2/CH4 separation using asymmetric mixed matrix membrane. *RSC Adv*. 2014;4(94):52530–52541. doi:10.1039/c4ra08460h
38. Zheng X, Ma Z, Zhang D. Synthesis of imidazole-based medicinal molecules utilizing the van Leusen imidazole synthesis. *Pharmaceuticals*. 2020;13(3):37. doi:10.3390/ph13030037
39. Wang Q, Sun Y, Li S, Zhang P, Yao Q. Synthesis and modification of ZIF-8 and its application in drug delivery and tumor therapy. *RSC Adv*. 2020;10(62):1. doi:10.1039/d0ra07950b
40. de Moura Ferraz LR, Tabosa AÉGA, da Silva Nascimento DDS, et al. ZIF-8 as a promising drug delivery system for benznidazole: development, characterization, in vitro dialysis release and cytotoxicity. *Sci Rep*. 2020;10(1):16815. doi:10.1038/s41598-020-73848-w
41. Burchmore RJS, Barrett MP. Life in vacuoles - Nutrient acquisition by Leishmania amastigotes. *Int J Parasitol*. 2001;31(12):1311–1320. doi:10.1016/s0020-7519(01)00259-4
42. Lee YR, Jang MS, Cho HY, Kwon HJ, Kim S, Ahn WS. ZIF-8: a comparison of synthesis methods. *Chem Eng J*. 2015;271:276–280. doi:10.1016/j.cej.2015.02.094
43. Sun CY, Qin C, Wang XL, et al. Zeolitic imidazolate framework-8 as efficient pH-sensitive drug delivery vehicle. *Dalton Trans*. 2012;41 (23):6906–6909. doi:10.1039/c2dt30357d
44. Chen P, He M, Chen B, Hu B. Size- and dose-dependent cytotoxicity of ZIF-8 based on single cell analysis. *Ecotoxicol Environ Saf*. 2020;205:111110. doi:10.1016/j.ecoenv.2020.111110

45. Leng X, Dong X, Wang W, et al. Biocompatible fe-based micropore metal-organic frameworks as sustained-release anticancer drug carriers. *Molecules*. 2018;23(10):2490. doi:10.3390/molecules23102490
46. Duan W, Qiao S, Zhuo M, et al. Multifunctional Platforms: metal-Organic Frameworks for Cutaneous and Cosmetic Treatment. *Chem*. 2021;7 (2):450–462. doi:10.1016/j.chempr.2020.11.018
47. Vasconcelos IB, Wanderley KA, Rodrigues NM, da Costa NB, Freire RO, Junior SA. Host-guest interaction of ZnBDC-MOF + doxorubicin: a theoretical and experimental study. *J Mol Struct*. 2017;1131:36–42. doi:10.1016/j.molstruc.2016.11.034
48. Tran VA, Lee SW. pH-triggered degradation and release of doxorubicin from zeolitic imidazolate framework-8 (ZIF8) decorated with polyacrylic acid. *RSC Adv*. 2021;11(16):9222–9234. doi:10.1039/d0ra10423j
49. Liu X, Wang Y, Yuan J, et al. Prediction of the Ibuprofen Loading Capacity of MOFs by Machine Learning. *Bioengineering*. 2022;9(10):517. doi:10.3390/bioengineering9100517
50. Faustino C, Pinheiro L. Lipid systems for the delivery of amphotericin B in antifungal therapy. *Pharmaceutics*. 2020;12(1):29. doi:10.3390/pharmaceutics12010029
51. Zheng H, Zhang Y, Liu L, et al. One-pot Synthesis of Metal-Organic Frameworks with Encapsulated Target Molecules and Their Applications for Controlled Drug Delivery. *J Am Chem Soc*. 2016;138(3):962–968. doi:10.1021/JACS.5B11720
52. Vasconcelos IB, Da Silva TG, Militão GCG, et al. Cytotoxicity and slow release of the anti-cancer drug doxorubicin from ZIF-8. *RSC Adv*. 2012;2 (25):9437–9442. doi:10.1039/C2RA21087H
53. Soltani B, Nabipour H, Nasab NA. Efficient Storage of Gentamicin in Nanoscale Zeolitic Imidazolate Framework-8 Nanocarrier for pH-Responsive Drug Release. *J Inorg Organomet Polym Mater*. 2018;28(3):1090–1097. doi:10.1007/s10904-017-0745-z
54. Tiwari A, Singh A, Garg N, Randhawa JK. Curcumin encapsulated zeolitic imidazolate frameworks as stimuli responsive drug delivery system and their interaction with biomimetic environment. *Sci Rep*. 2017;7(1). doi:10.1038/s41598-017-12786-6
55. Nimtrakul P, Williams DB, Tiyaboonchai W, Prestidge CA. Copolymeric micelles overcome the oral delivery challenges of amphotericin B. *Pharmaceuticals*. 2020;13(6):121. doi:10.3390/ph13060121
56. Agarwal A, Kar BR. Amphotericin-B in Dermatology. *Indian Dermatol Online J*. 2022;13(1):152–158. doi:10.4103/idoj.idoj_573_21
57. Fernández-García R, Muñoz-García JC, Wallace M, et al. Self-assembling, supramolecular chemistry and pharmacology of amphotericin B: poly-aggregates, oligomers and monomers. *J Control Release*. 2022;341:716–732. doi:10.1016/j.jconrel.2021.12.019
58. Alvarez C, Shin DH, Kwon GS. Reformulation of Fungizone by PEG-DSPE Micelles: deaggregation and Detoxification of Amphotericin B. *Pharm Res*. 2016;33(9):2098–2106. doi:10.1007/s11095-016-1948-7
59. Oyewumi MO, Kumar A, Cui Z. Nano-microparticles as immune adjuvants: correlating particle sizes and the resultant immune responses. *Expert Rev Vaccines*. 2010;9(9):1095–1107. doi:10.1586/erv.10.89
60. Gomes FL, Conceição F, Teixeira LM, Leijten J, Jonkheijm P. Production of Hydrophobic Microparticles at Safe-To-Inject Sizes for Intravascular Administration. *Pharmaceutics*. 2025;17(1):64. doi:10.3390/pharmaceutics17010064
61. Svirkin Y, Lee J, Marx R, et al. Amphotericin B release rate is the link between drug status in the liposomal bilayer and toxicity. *Asian J Pharm Sci*. 2022;17(4):544–556. doi:10.1016/j.ajps.2022.04.007
62. Díaz de León–Ortega R, D'Arcy DM, Lamprou DA, Xue WF, Fotaki N. In vitro in vivo relations for the parenteral liposomal formulation of Amphotericin B: a biorelevant and clinically relevant approach. *Eur J Pharm Biopharm*. 2021;159:188–197. doi:10.1016/j.ejpb.2020.07.025
63. Espada R, Valdespina S, Alfonso C, Rivas G, Ballesteros MP, Torrado JJ. Effect of aggregation state on the toxicity of different amphotericin B preparations. *Int J Pharm*. 2008;361(1–2):64–69. doi:10.1016/j.ijpharm.2008.05.013
64. Hussain A, Samad A, Singh SK, et al. Nanoemulsion gel-based topical delivery of an antifungal drug: in vitro activity and in vivo evaluation. *Drug Deliv*. 2016;23(2):642–657. doi:10.3109/10717544.2014.933284
65. Tang J, Srinivasan S, Yuan W, et al. Development of a flow-through USP 4 apparatus drug release assay for the evaluation of amphotericin B liposome. *Eur J Pharm Biopharm*. 2019;134:1. doi:10.1016/j.ejpb.2018.11.010
66. Huang Z, Dong P, Zhang Y, Nie X, Wang X, Zhang X. A ZIF-8 decorated TiO2 grid-like film with high CO2 adsorption for CO2 photoreduction. *J CO2 Util*. 2018;24:369–375. doi:10.1016/j.jcou.2018.01.024
67. Zhang Y, Jia Y, Hou L. Synthesis of zeolitic imidazolate framework-8 on polyester fiber for PM2.5 removal. *RSC Adv*. 2018;8(55):31471–31477. doi:10.1039/c8ra06414h
68. Lukić M, Pantelić I, Savić SD. Towards optimal ph of the skin and topical formulations: from the current state of the art to tailored products. *Cosmetics*. 2021;8(3):69. doi:10.3390/cosmetics8030069
69. Layegh P, Rajabi O, Jafari MR, et al. Efficacy of topical liposomal amphotericin B versus intralesional meglumine antimoniate (Glucantime) in the treatment of cutaneous leishmaniasis. *J Parasitol Res*. 2011;2011:656523. doi:10.1155/2011/656523
70. Boshrouyeh R, Amari S, Boshrouyeh Ghandashtani M, Alavi SE, Ebrahimi Shahmabadi H. A topical gel nanoformulation of amphotericin B (AmB) for the treatment of cutaneous leishmaniasis (CL). *J Sol-Gel Sci Technol*. 2023;105(3):768–780. doi:10.1007/s10971-023-06041-w
71. Jaafari MR, Hatamipour M, Alavizadeh SH, et al. Development of a topical liposomal formulation of Amphotericin B for the treatment of cutaneous leishmaniasis. *Int J Parasitol Drugs Drug Resist*. 2019;11:156–165. doi:10.1016/j.ijpddr.2019.09.004
72. Bigham A, Islami N, Khosravi A, Zarepour A, Iravani S, Zarrabi A. MOFs and MOF-Based Composites as Next-Generation Materials for Wound Healing and Dressings. *Small*. 2024;20(30). doi:10.1002/SMLL.202311903
73. Chen Y, Li Y, Song H, et al. Injectable Nanocomposite Hydrogel for Accelerating Diabetic Wound Healing Through Inflammatory Microenvironment Regulation. *Int J Nanomed*. 2025;20:1679–1696. doi:10.2147/IJN.S505918
74. Xiang Y, Huang S, Tang D, et al. MOF/polypeptide hybrid nanocomposites with pH/lipase dual responsive drug release and photodynamic effect for combination treatment of drug-resistant bacterial infection. *Mater Des*. 2023;232:112180. doi:10.1016/j.matdes.2023.112180